Temperature Compensation to Guided Wave-based Monitoring of Bolt Loosening Using An Attention-based Multi-task Network

Fei Du[1,2*], Shiwei Wu[1], Sisi Xing[3,1] , Chao Xu[1,2], Zhongqing Su[4,1]

[1]School of Astronautics, Northwestern Polytechnical University, Xi'an, 710072, China

[2]Yangtze River Delta Research Institute of Northwestern Polytechnical University, Taicang, 215400, China

[3]Xian Aerospace Propulsion Institute, Xi'an, 710100, China

[4]Department of Mechanical Engineering, The Hong Kong Polytechnic University, Kowloon, Hong Kong Special Administrative Region

*Corresponding authors. E-mail: dufei@nwpu.edu.cn

Highlights:

(1) An attention-based multi-task network is developed for accurate detection of bolt loosening in multi-bolt connections over a wide range of temperature variation.

(2) The Integrated Gradients method and a simplified structure of the bolt lap plate are used to interpret the multi-task network.

(3) It has been proven that the A_0 mode is sensitive to bolt loosening, while the S_0 mode is not.

(4) The generalization capabilities of the multi-task network have been verified.

Abstract:

Online monitoring of bolt torque is critical to ensure the safe operation of bolted structures. Guided waves have been intensively explored for bolt loosening monitoring. Nevertheless, guided waves are excessively sensitive to fluctuation of ambient temperature. As a result of the complexity of wave transmitting across a bolted joint, it is highly challenging to compensate for the effect of temperature. To this end, an attention-based multi-task network is developed towards accurate detection of bolt loosening in multi-bolt connections over a wide range of temperature variation. By integrating improved attention gate modules in a modified U-Net architecture, an attention U-Net is configured for temperature compensation. A two-layer convolutional subnetwork is connected in series behind the attention U-Net to identify bolt loosening. Experimental validation is carried out on a bolt jointed lap plate simulating a real aircraft structure. The results have proved that the developed multi-task network achieves temperature compensation and accurate bolt loosening identification. To further understand the multi-task network, the Integrated Gradients method and a simplified structure of the bolt lap plate are used to interpret the developed network. It is proved that the A_0 mode is sensitive to bolt loosening, while the S_0 mode is not.

Keywords: bolt loosening monitoring, guided wave, temperature compensation, attention gate, multi-task network.

1. Introduction

Bolted joints are widely used to hold different parts together in aerospace and civil structures, since they are easy to assemble and have a strong bearing capacity. However, the bolted joints are easy to lose their preloads due to improper installation, external loading, and temperature effect[1][2]. Bolt connection looseness will reduce structural reliability and even cause structural failure. Therefore, it is critical to monitor bolt looseness online to ensure the safe operation of bolted structures[3].

Guided waves have been intensively explored in the field of structural health monitoring(SHM)[4], because it has the advantages of large monitoring area and high sensitivity to small damages in structures[5][6]. In recent years, a great number of studies focused on the detection of bolt loosening using guided waves have been carried out[7]. Due to the complex structure of the bolted joint, guided wave mode conversion is more complicated and the captured signals present higher multi-modal. The general method based on wave packages is invalid[4]. Yang and Chang[8] proposed to use the energy and attenuation speed of guided wave transmitted across the bolt jointed interface to assess preload levels and locations of loosening bolt in thermal protection panels in space vehicles. Since then, the transmitted guided wave energy is widely used as a tightness index because the wave energy across the bolt joint is strongly tied to the contact status of bolted interface[7][9][10].

To identify bolt loosening in a test structure of a CubeSat, Mascarenas et al.[11] used the difference in transmitted guided wave energy between the operational measurements and the baseline measurements to locate loosening bolts. Similarly, Montoya et al.[12] proposed to detect loosening bolts in a single joint between satellite panels using transmitted guided wave energy. Jiang et al.[13] developed a guided wave approach based on wavelet packet energy analysis to access bolt looseness in steel truss arch structures. Recently, Zhu et al.[4] proposed a guided wave method to measure the preload between rotor disks based on the wave energy. However, the guided wave energy based approach is not sensitive at the early stage of bolt loosening[14][15]. Therefore, the above research is limited to the monitoring of fully loosening bolt in multi-bolt

connection. Parvasi et al.[16] developed a time reversal method to monitor bolt preload, in which the time reversal technique was used to focus the energy of transmitted guided wave. Moreover, Du et al.[14] proposed a modified time reversal method that is more sensitive to bolt loosening. Wang et al.[15] develop a new entropy-based tightness index for monitoring bolt early looseness.

The temperature effect is among the major environmental influences that can restrict real-life SHM applications of guided wave[17]. The characteristics of wave propagation like wave velocities, amplitudes change with temperature[17]. Therefore, it is important to compensate for the effect of temperature on guided waves for practical application. Lu and Michaels [18] and Konstantinidis et al.[19] illustrated optimal baseline selection (OBS) methods for temperature compensation. The OBS method is based on the identification of a signal within a database that is most similar to a current signal. Based on the OBS method, An and Sohn[20] presented an integrated impedance and guided wave method for damage detection under varying temperature conditions. However, significant changes in signals will happen with very small temperature drifts, which means the temperature interval between baselines should be very small[21]. As the dominant effect of temperature is the change in arrival time of individual wave packets, baseline signal stretch (BSS) methods have been proposed[18, 22]. In BSS, the signal was stretched or compressed by modifying its time or frequency axis to compensate for this time delay. Recently, Mariani et al. [23] presents a new stretch-based temperature compensation procedure allowing for both wave velocity and transducer phase response changes. For anisotropic composite structure, Yue and Aliabadi [24] proposed a stretch-based method to compensate for both wave phases and amplitudes at various temperatures. Nevertheless, the success of the stretch-based methods is strongly dependent on mode purity and structural complexity[25], since the stretch factor changes with wave mode and frequency. Therefore, the BSS method is difficult to apply to guided waves received from bolted joints in which the overlapping between different mode waves is more common. Until now, few studies have considered the temperature effect in bolt loosening detection based on guided waves.

Machine learning (ML) techniques have been used for bolt loosening detection due

to their capabilities of modeling extremely complex nonlinear phenomena. Nazarko and Ziemianski[26] proposed to use principle components analysis (PCA) and artificial neural networks(ANN) for bolt force identification based on elastic waves. Furthermore, Liang and Yuan[27] developed a decision fusion system for bolted joint monitoring based on Lamb waves. Recently, Wang et al.[28] developed a new damage index (DI) and a least square support vector machine (SVM) was used to identify different loosening states of a multi-bolt connection. After that, Wang et al.[29] further presented new entropy indexes and a stacking-based ensemble learning classifier to detect underwater multi-bolt looseness using guided waves. It can be seen that ML methods are increasingly used for loosening monitoring of multi-bolt connection structures due to the complexity of the guided wave signals. However, the accuracy of the ML techniques relies on the effectiveness of the features extracted from guided wave signals [17].

ML techniques have also been attempted to remove the temperature effect. To detect damage in a steel pipe under environmental variations, Ying et al. [30] proposed to use automated feature selection and ML classifiers for damage classification. Wang et al.[31] present a PCA based method to eliminate the temperature effects for ice monitoring of wind turbine blade. However, it is very difficult to find a universally good feature that is sensitive to complex loosening conditions, while robust in the presence of temperature variations.

In recent years, deep learning has brought about breakthroughs in processing images, video, audio and natural language[32]. It performs much better than traditional handcrafted feature-based ML methods among lots of tasks. Recently, deep learning techniques have been increasingly used in the field of SHM[33-37]. Zhang et al. [38] presented a faster region-based convolutional neural network(CNN) for bolt loosening detection using machine vision. Wang and Song[1] developed a one-dimensionaltraining interference capsule neural network (1D-TICapsNet) to classify percussion-induced sound signals for bolt looseness detection. Wang[39] further developed a novel robotic-assisted active sensing method and a new Siamese CapsNet for multi-bolt loosening detection. Zhang et al.[40] proposed a CNN, namely SHMnet, for bolt loosening identification using vibration signals. Multi-task learning based deep neural networks

are suitable for solving the problem of multi-task detection. Hence, Zhang et al.[41] developed a multi-task CNN for simultaneous detection of damage level and location using lamb wave. Though considerable research has been conducted in the application of ML in SHM, the implementation of deep learning techniques in Lamb wave based bolt loosening detection is still limited.

From the above analysis, it can be seen that guided wave is effective for bolt torque monitoring. However, due to the complexity of the guided wave transmitting across a bolted joint, few studies have considered the effect of temperature. The idea of self-attention mechanisms is to generate a context vector that assigns weights to the input sequence. The self-attention mechanisms were first popularized in natural language processing[42]. In computer vision, self-attention has been applied to a variety of tasks, including image classification[43], segmentation[44-46] and image synthesis[47]. For medical imaging segmentation, Oktay et al.[45] proposed a self-attention module named attention gates (AGs) which can progressively suppress feature responses in irrelevant background regions and preserve only the activations relevant to the specific task. Based on the AG, Abraham and Khan[46] further improved the attention U-Net by incorporating an image pyramid for small lesion segmentation. Inspired by this, an attention-based multi-task network is developed in this paper towards accurate detection of bolt loosening over a wide range of temperature variation. The multi-task network consists of an improved attention U-Net subnetwork for temperature compensation, and a two-layer convolutional subnetwork to identify bolt loosening states. The generalization capability of the proposed multi-task network is verified experimentally. To further understand the decisions, the developed multi-task network is interpreted by the Integrated Gradients method and a simplified structure of the bolt lap plate.

The content of this paper is arranged as follows. Section 2 introduces the theoretical background of bolt loosening detection using guided waves and the effect of temperature. Section 3 presents the attention-based multi-task network. The experiment is shown in section 4. Section 5 displays the experimental results and the generalization capability of the multi-task network. In section 6, the network is interpreted. The study

is concluded in section 7.

2．Fundamental of Guided Wave Monitoring

2.1 Guided wave monitoring of bolt torque

Lead zirconate titanate (PZT) is widely used for guided wave excitation. Two PZT sheets can be attached to both sides of a bolt joint, one for excitation and the other for reception. Then, the bolt preload can be estimated by the change of the received guided wave signal, as shown in Fig. 1.
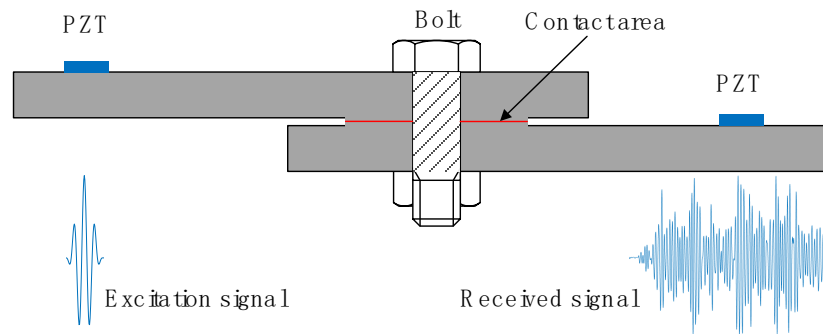

Figure 1 Schematic diagram of guided wave propagation across a bolted joint

The relationship between the given tightening torque and the arising pretension force can be described by.

$$T = Fkd \tag{1}$$

where F, T, k and d are the pretension force, the tightening torque, the torque coefficient and the nominal diameter of the bolt, respectively. As the torque increases, the bolt pretension force increases. At this time, the contact area between the two connecting plates also increases. On macro level, this is caused by the increase of the radius of nominal contact area around the bolt [48, 49]. On the micro-scale, this phenomenon is associated with the increase of the true contact area between the contact asperities[9]. The change in the contact area between the plates causes a change in the wave propagation signal[50].

In reality, an actual received guided wave signal contains mode conversions and scattering waves at the contact interface and the bolt hole, as well as reflections at the ends of the lapped plates. As a result, the received guided wave signal exhibits complicated patterns, as shown in Fig. 1. The energy of the transmitted guided wave is

usually used as the bolt loosening index [8, 9, 51]. The signal energy in the discrete time domain [t_s, t_f] can be calculated by：

$$E = \sum_{t=t_s}^{t_f} V^2(t) \tag{2}$$

where $V(t)$ is the voltage signal of the received guided wave.

2.2 The effect of temperature on guided waves

Temperature fluctuations cause changes in the material properties of the structure, the piezoelectric sensor and the bonding layer, as well as changes in their dimensions. In general, such a temperature shift may alter the shape, amplitude and arrival time of each individual wave packet. However, to a first approximation, the dominant effect is the change in arrival time of individual wave packet [52]. The shift of arrival time can be calculated by[53]:

$$\delta t = \frac{L}{v_p}\left(\alpha - \frac{k_T}{v_p}\right)\delta T \tag{3}$$

where δT is the variation in temperature, L is the propagation distance, v_p is the phase velocity, α is the coefficient of thermal expansion, and k_T is the coefficient of change in phase velocity with temperature. Note that the size of k_T/v_p is typically one to two orders of magnitude larger than α. Therefore, the effect of the thermal expansion of the structure can be ignored[53].

It can be seen that the phase velocity and propagation distance of the guided wave have significant effects on the signal variation. Therefore, the influence of temperature on guided waves of different modes is different. Eq. 3 is only applicable to the guided wave packet containing a single mode. For guided waves across a bolt jointed, it is difficult to compensate the temperature effect by the commonly used BSS technique which is strongly dependent on mode purity.

3 . Attention-based multi-task network considering temperature variation

In this section, a multi-task network based on the self-attention mechanism is built to implement temperature compensation and loosening state recognition.

3.1 An improved Attention Gate

The self-attention mechanism can dynamically generate different connection weights, and long-range dependencies can be modeled. The architecture of the conventional AG presented by Oktay et al.[45] is shown in Fig. 2a. However, the module is for medical image segmentation[46], while this paper is for wave signal regression. Therefore, an improved 1D AG module is proposed for guided wave processing and the architecture is shown in Fig.2b.
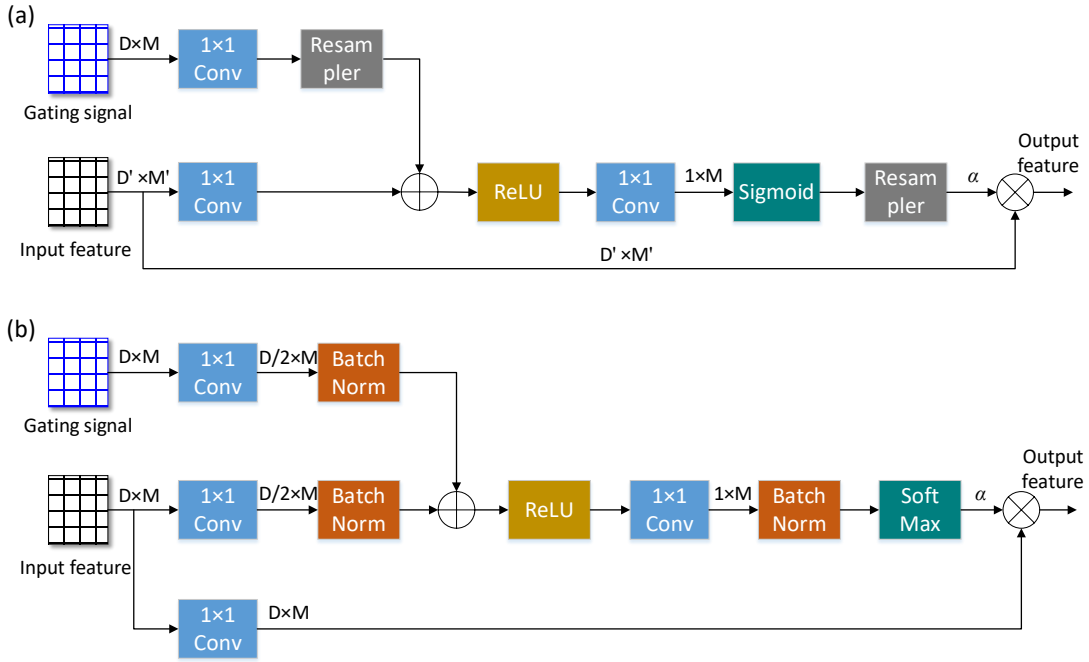

Figure 2 The AG modules (a) the conventional AG[45, 46] (b) the improved AG

In Fig. 2, D and D' are the numbers of channels, and M and M' are the lengths of the signals. α is the element-wise attention coefficient. The $\oplus$ denotes element-wise add and the $\otimes$ denotes element-wise multiplication. In the AG modules, the gating signals are from higher-level features and the input features are from lower-level features. The gating signals contain contextual information to prune input feature responses. Compared with the conventional AG, the following improvements are made in the improved AG for the wave signal regression, as shown in Fig. 2b.

(1) A linear transformation of 1×1 convolution is added before the input features are scaled with attention coefficients.

(2) The softmax activation function is used to normalize the attention coefficients.

(3) The conventional AG uses linear interpolation as resampling. In the improved AG, the gating signals are from the outputs of the transposed convolutions in the expansive path. Hence, there is no resampling.

(4) The batch normalization layers are added to train the AG module faster and more stably.

3.2 A 1D attention U-Net for temperature compensation

By integrating the improved AG modules in a modified U-Net architecture[54], a 1D attention U-Net is established for guided wave temperature compensation at various damage states. This network is named the compensation subnetwork (Comp-net). The architecture of the Comp-net is shown in Fig. 3. In addition, the numbers of channels are also displayed in Fig. 3. With more channels, more features can be extracted by the convolutional layers. But this also leads to more parameters for the network. The performance of the network with different number of channels was compared. The results showed that the number of channels shown in Fig.3 can provide the best performance.
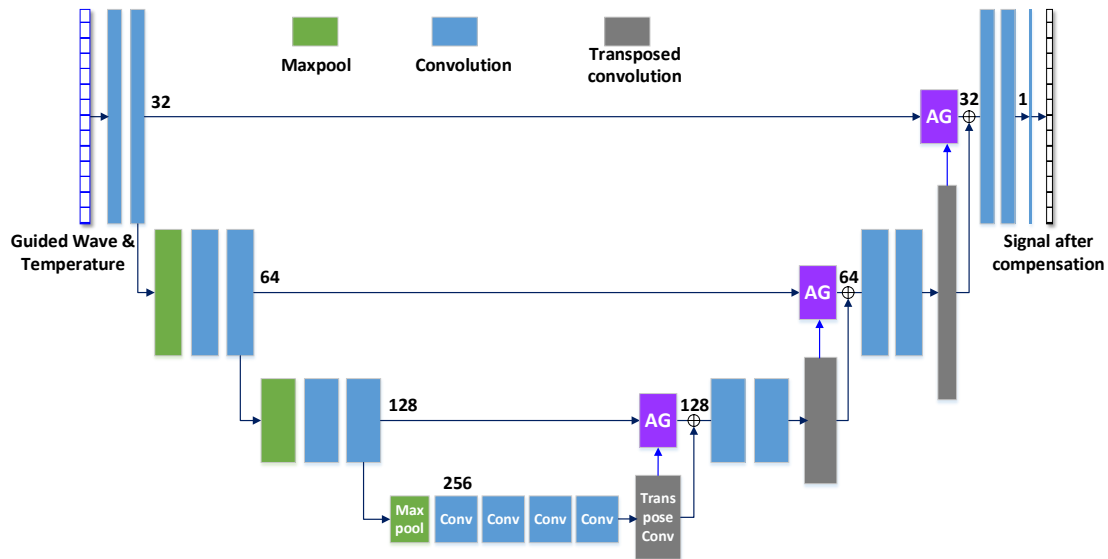

Figure 3 The temperature compensation subnetwork

The input features of the Comp-net have two channels, the first channel is the guided wave signal vector and the second channel is the corresponding temperature vector. The temperature is expanded so that its length is the same as the guided wave signal. Hence, each element has the same value in the temperature vector. In the

contracting path, the convolution layers are used to extract features from a local region, and three max pooling layers are used for downsampling. In the expansive path, three transposed convolutional layers, which are transposed forms of convolution operation, are used for trainable upsampling.

In the AG modules, higher-level features from the outputs of the transposed convolutions in expansive path are used as the gating signals to highlight relevant lower-level features that are derived from the contracting path. After that, the output features of the AG modules are directly added to the higher-level features. Note that this addition operation is different from the concatenation operation in the standard U-Net. In addition, the batch normalization layer is not used in the Comp-net except the AG module. These changes result in better performance of the Comp-net.

3.3 A multi-task network for bolt loosening state identification

Multi-task learning aims to jointly learn multiple related tasks and has been used successfully across many applications of machine learning. Multi-task learning improves generalization by leveraging the domain-specific information contained in the training signals of related tasks[55]. On the basis of the Comp-net, a multi-task network for bolt loosening state identification is developed by connecting a classification subnetwork(Class-net) in series behind the Comp-net. The architecture of the attention-based multi-task network is displayed in Figure 4.

The Class-net is very simple which consists of two convolutional layers, two pooling layers and a fully connected layer. Moreover, a skip connection is used to concatenate the input guided wave signal and the signal after compensation. And these two-channel features are used as the input of the Class-net. The output of the Class-net is the identified bolt loosening state. Hence, in the multi-task network, there are two outputs: the compensated guide wave signal and bolt loosening state.
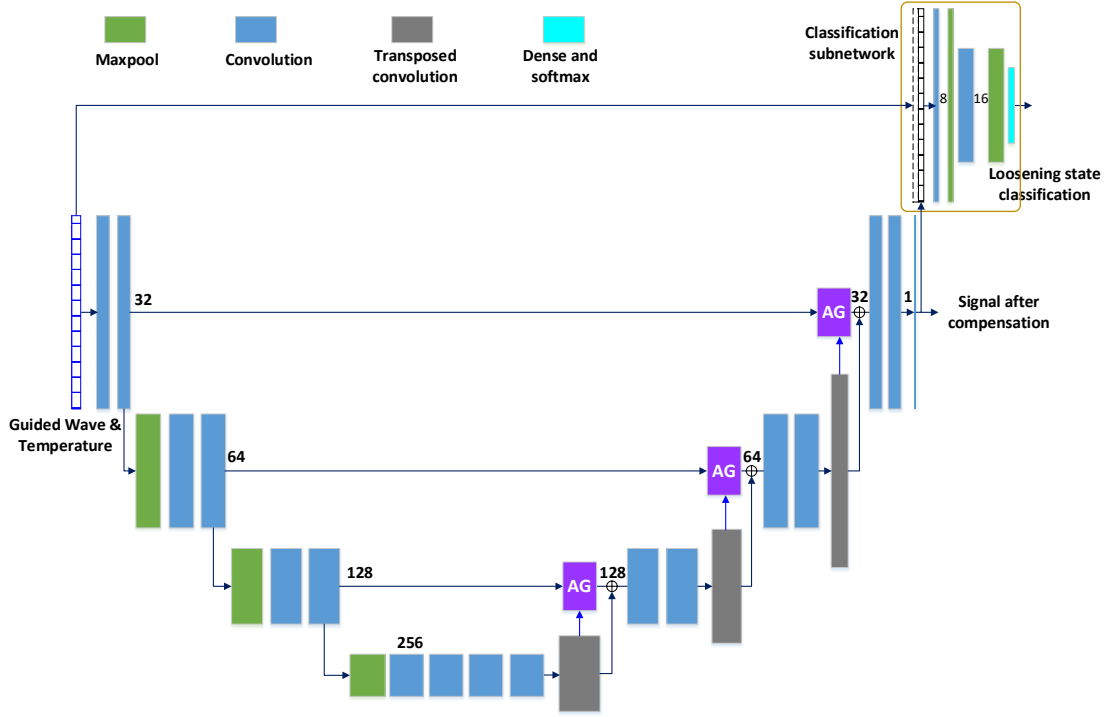
Figure 4 The architecture of the proposed multi-task network

3.4 Loss function

For the Comp-net, the loss function shown in the following equation is used.

$$\mathcal{L}_1 = \mathcal{L}_{\text{MSE}} + \lambda_{\text{TV}}\mathcal{L}_{\text{TV}} \tag{4}$$

where $\mathcal{L}_{\text{MSE}}$ is the mean squared error loss which measures the average squared difference between the actual and compensated guided wave signals, λ_{TV} is the tradeoff parameter, and $\mathcal{L}_{\text{TV}}$ is the total variation (TV) regularizer which can be used to constrain the smoothness of the difference between the actual and compensated guided wave signals[56]. For 1D signals, $\mathcal{L}_{\text{TV}}$ can be written as:

$$\mathcal{L}_{TV} = \sum_{i=1}^{M-1}(d_{i+1} - d_i)^2/(M-1) \tag{5}$$

where M is the length of the signal and d is the difference between the actual and compensated values.

The loss function of the multi-task network is[54]

$$\mathcal{L} = \beta\mathcal{L}_1 + (1-\beta)\mathcal{L}_2 \tag{6}$$

where $\mathcal{L}_2$ is the cross-entropy loss for the Class-net, β is the tradeoff parameter for $\mathcal{L}_1$.

4. Experimental validation

To validate the attention-based multi-task network, experiments were carried out

using a lap aluminum plate jointed by 24 bolts simulating an aircraft structure. The parameters including plate thickness, lap width, as well as bolt size and spacing were determined according to a real aircraft structure. Two PZTs were used to monitor the tightening toques of six bolts over a wide range of temperature variation. Three different training and validation data sets were built using the measured guided wave signals.

4.1 Specimen and experimental setup

The specimen of the bolt jointed lap plate used in the experiment is shown in Figure 5. The bolts are steel M6 bolts with strength class 8.8, and flat washers were used in each bolt. The two aluminum plates were lapped using 24 bolts, and the size of each aluminum plate is 380×266 mm.
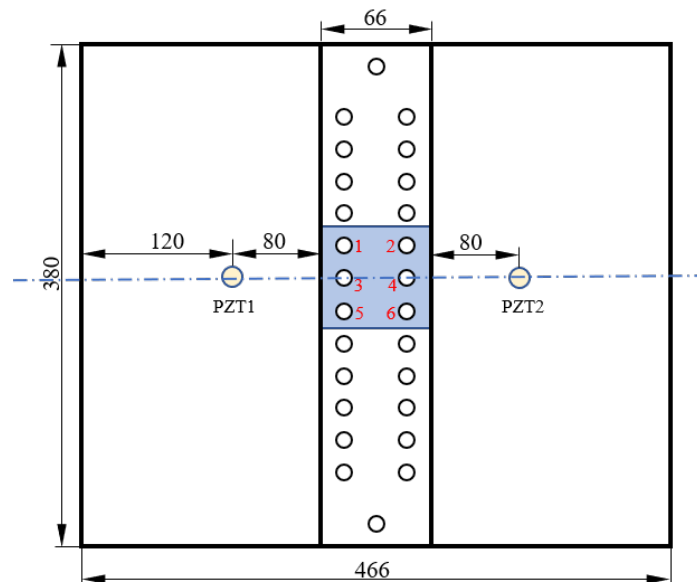

Figure 5 Schematic diagram of the 24-bolt lap plate

Two PZT sensors were glued to the two sides of the bolts in the specimen. PZT 1 was used to excite a guided wave and PZT 2 was used to receive the guided wave signal. The material of the PZTs is P5-1, and the size is $\phi8$ mm$\times$0.5 mm. The excitation signal was a Hanning window modulated 3.5-period sine signal with a center frequency of 150 kHz. A NI PXIe-5413 was used to excite PZT 1 and a NI PXIe-5105 was used to acquire the guide wave signal received by PZT 2 with a sampling frequency of 20 MHz.

A STANLEY SD-030-22 torque wrench was used to tighten the M6 bolts to a predetermined torque. Different loosening states of the six bolts shown in Figure 5 were monitored, while the other bolts were always kept tight (8Nm). A total of 13 bolt

loosening states were measured in the experiments, as listed in Table 1.

Table 1 The loosening states in the experiment

Loosening state	Torques of the six bolts
1	No.1 0Nm，others 8Nm
2	No.1 4Nm，others 8Nm
3	No.2 0Nm，others 8Nm
4	No.2 4Nm，others 8Nm
5	No.3 0Nm，others 8Nm
6	No.3 4Nm，others 8Nm
7	No.4 0Nm，others 8Nm
8	No.4 4Nm，others 8Nm
9	No.5 0Nm，others 8Nm
10	No.5 4Nm，others 8Nm
11	No.6 0Nm，others 8Nm
12	No.6 4Nm，others 8Nm
13	all 8Nm

Two temperature controller of ESS-SH050A and GDW-50 were used for high and low temperature experiments, respectively. The temperature controller of ESS-SH050A does not have the cooling function. The specimen temperatures were accurately measured by a FLUKE 17B+ digital multimeter. For the high temperature experiment, the temperature range is from 23°C to 51°C. For the low temperature experiment, the temperature range is from -16.2°C to 35°C. The reference temperature is 30±0.1°C for each loosening state. The temperature distribution is not exactly the same for all loosening states.

4.2 Data sets for training and validation

For each loosening state, a specific bolt was completely loosened, and then tightened to the predetermined torques. After that, a temperature controller was used to heat or cool and hold a desired temperature for 15 minutes. In this way, guided wave samples were measured at different temperatures. This process was named a tightening batch and was repeated. In the high temperature experiment, there are 3 tightening batches for each loosening state. In addition, there are 15 samples in one tightening

batch, and 45 samples in one loosening state. The total number of samples in the high temperature experiment is 585. The temperature distribution in the high temperature experiment is shown in Fig. 6a. There are 10 different temperatures, 2.5 degrees apart. In the low temperature experiment, there are 2 tightening batches for each loosening state. There are 22 samples in one tightening batch, and 44 samples in one loosening state. The total number of samples in the low temperature experiment is 572. The temperature distribution is shown in Fig. 6b. There are 11 different temperatures, 5 degrees apart.
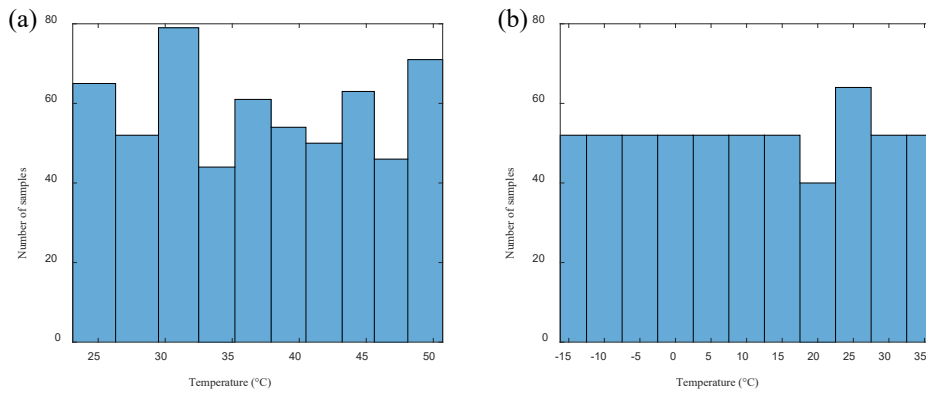

Figure 6. The temperature distribution of the samples (a) high temperature experiment (b) low temperature experiment

It can be seen that the temperature distribution of the samples is basically uniform. 20% of the samples in a loosening state were randomly selected as the validation set, and the remaining 80% were used as the training set. In this way, there are 936 samples in the training set and 221 samples in the validation set. This data set is named the "Normal temperature data set".

For a specific bolt loosening state, different bolt tightening batches lead to variations in the guided waves even if the corresponding temperatures are the same. Hence, the generalization capability of the proposed multi-task network for different tightening batches was verified. For each bolt loosening state, 3 batches were used for training and the other 2 batches was used for validation. Note that the two batches obtained by the temperature controller GDW-50 were in the training and validation sets, respectively. Therefore, there are 676 samples in the training set and 481 samples in the

validation set. This data set is named the "Tightening batch data set".

In practice, the ambient temperature may not be within the training temperature range. In this case, the generalization capability of the proposed multi-task network is investigated. For each bolt loosening state, samples in the temperature range from -5°C to 45 °C were used for training, and samples in the ranges from -16.2°C to -5°C and from 45°C to 50°C were used for validation. At this time, there are 922 samples in the training set and 235 samples in the validation set. This data set is named the "Abnormal temperature data set".

4.3 Training strategy and hyperparameters

In the model training, the input guided wave was normalized by the Z-score normalization method. To normalize the temperature, the difference between the measured temperature and the reference temperature was divided by 10, and then the result was used as the temperature input.

The network was built and trained using the Pytorch platform. For the training of the multi-task network, the Adam optimization algorithm was used, and the hyperparameters used are listed in Table 2. The learning rate changes dynamically during the training process.

Table 2 The hyperparameter values

Hyperparameter	Values
λ_{TV}	0.02
β	0.8
Epoch	120
Batch size	9
Initial learning rate	2e-3

5．Experimental results

The results of temperature compensation and bolt loosening state recognition are displayed in this section. In addition, the generalization ability of the proposed model is verified. Moreover, the effects of the AG module and the skip connection between the two subnetworks are investigated. Finally, the above results are compared with the

results of the SHMnet[40], and the effect of temperature compensation is discussed.

5.1 Temperature compensation and loosening state recognition

In the experiment, it is necessary to select the length of the input guided wave signal. To this end, signals of lengths 25 μs, 50 μs, 75 μs, and 100 μs were selected, as shown in Fig. 7a. Note that T_0=45 μs is used as the starting point of the input guided wave signal.
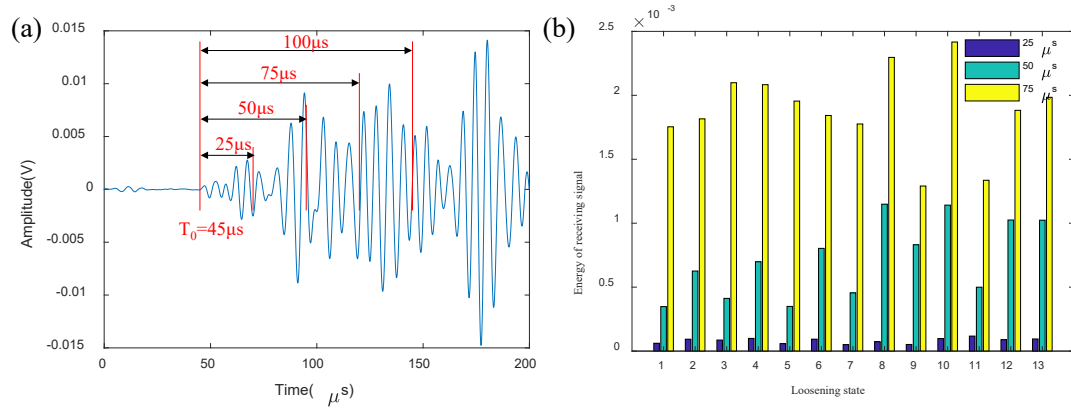

Figure 7. The received guided wave signal (a) Schematic diagram of signal length (b) Signal energy in different loose states at the reference temperature

The variations of the energy of the 25 μs, 50 μs and 75 μs signals with the loosening states at the reference temperature were calculated, as shown in Fig. 7b. It can be seen that although the torques of the six bolts in loosening state 13 are all maximum, the energy of their signals is smaller than the energy of the signals of loosening state 8 and 10. It can be concluded that the loosening states cannot be distinguished by the energy of the received guided waves, even though there is no temperature effect.

The multi-task network was trained and validated using the Normal temperature data set. When the signal length is 75 μs, the loss and classification accuracy changes in a training process are shown in Fig. 8. The training is repeated three times. The average classification accuracy of the validation set is 100%, and the standard deviation is 0%, as listed in Table 3.
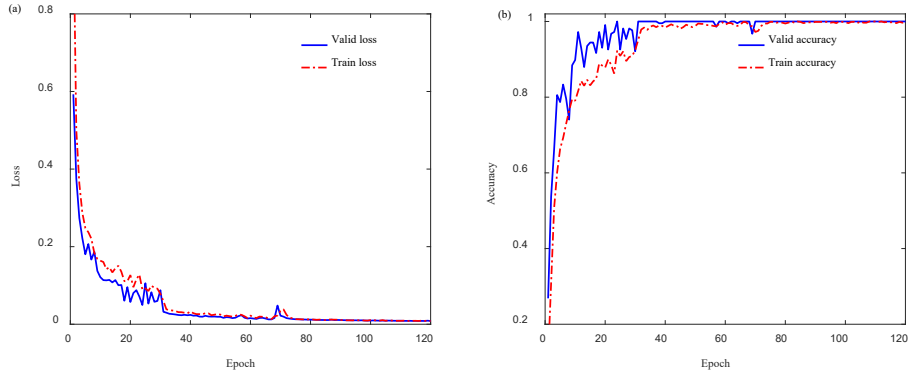
Figure 8. A training process of the multi-task network (a) Loss (b) Classification accuracy

When the signal lengths of 25, 50 and 100 μs were used, the classification accuracy of the verification set are shown in Figure 9. It can be seen that when the length is 75 μs, the accuracy is the highest. When the length is 25 μs, the accuracy is the lowest, only 90.2%. When the length is 50 μs and 100 μs, the accuracy is 98.1% and 99.5%, respectively. It can be seen that if the guided wave signal is too long or too short, the classification accuracy will be reduced. The reason will be analyzed in Section 6.
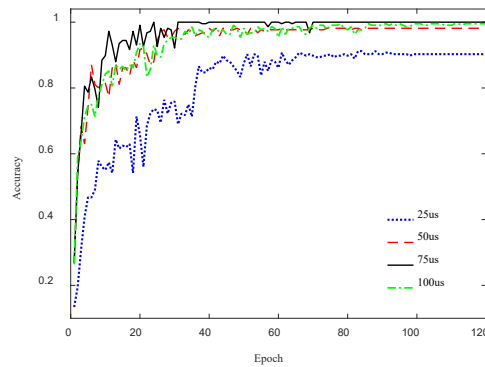

Figure 9 Validation accuracy of the multi-task network trained with different signal lengths

When the signal length is 75 μs, the compensated guided wave signals output from the Comp-net are shown in Fig. 10. They are also compared with the uncompensated guided wave signals and the signals measured at the reference temperature.
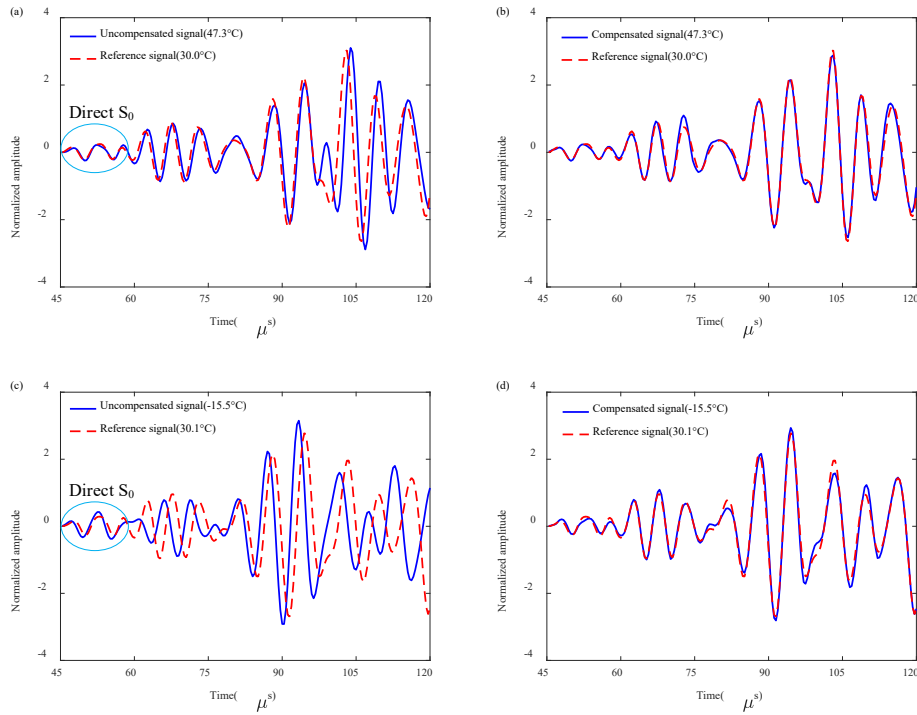
Figure 10 Temperature compensation results (a) uncompensated signal (47.3°C) in loosening state 4 (b) compensated signal (47.3°C) in loosening state 4 (c) uncompensated signal (-15.5°C) in loosening state 10 (d) compensated signal (-15.5°C) in loosening state 10.

As can be seen in Fig. 10, the compensated signal output from the Comp-net matches well with the signal measured at the reference temperature. It is proved that the proposed Comp-net can achieve temperature compensation well. At the same time, it can be seen that with the temperature change, the change of the guided wave signal is mainly time delay, especially before about 90 μs. This is consistent with the theoretical analysis in Section 2.2. It can be seen that the time delay of the signal shown in Fig. 10(c) is larger than that of the signal shown in Fig. 10(a). The main reason is that the temperature in Fig. 10(c) is 45°C different from the reference temperature. In contrast, the temperature in Fig. 10(a) is 17.3°C different from the reference temperature. On the other hand, the delay of the wave packets in the range of 45-60 μs in Fig. 10(c) is significantly reduced compared to other wave packets in Fig. 10(c). The main reason is that the time delay of S_0 wave is smaller than that of A_0 wave according to Eq. 3.[53] Therefore, the wave packet in the range of 45 - 60 μs is the first direct S_0

wave, and the subsequent wave packets have A_0 waves. At about 100 μs, the waveform of the guided wave changes considerably as the temperature changes. This is mainly due to the mode conversions as well as the different propagation paths of the guided wave across the bolted joint. The temperature has different effects on the guided waves with different propagation paths and different modes.

5.2 Generalization of the multi-task network

The generalization capability of the network has an important impact on its practical application. To this end, the proposed multi-task network is trained by the Tightening batch data set and the Abnormal temperature data set to verify its generalization capabilities for tightening batches and temperatures, respectively.

5.2.1 Generalization capability for tightening batches

Figure 11 shows the measured signals in different tightening batches of the loosening state 12 at the reference temperature. In Fig. 11, tightening batches 1 and 3 are from the high temperature experiment, and tightening batch 5 is from the low temperature experiment. It can be seen that, there are obvious differences in the measured signals of different tightening batches, although the loosening state and temperature are the same.
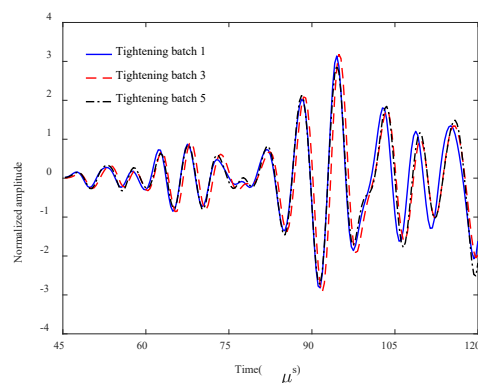

Figure 11 Guided wave signals of different tightening batches in the loosened state 12 at the

reference temperature

The multi-task network was trained and validated by the Tightening batch data set. The loss and classification accuracy changes in a training process are shown in Fig. 12.
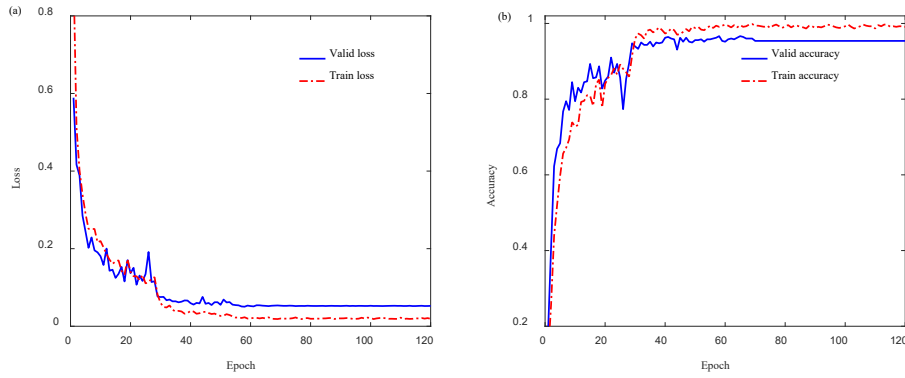
Figure 12. A training process using the Tightening batch data set (a) Loss (b) Accuracy

The training is repeated three times, and the mean value of validation accuracy was 95.60% with a standard deviation of 1.37%, as listed in Table 3. It is proved that the proposed network has good generalization capability for tightening batch. Compared with the results of the Normal temperature dataset, the classification accuracy on the Tightening batch data set decreases slightly, and the standard deviation increases slightly.

5.2.2 Generalization capability for temperature

The multi-task network was then trained and validated by the Abnormal temperature data set. The loss and classification accuracy changes in a training process are shown in Fig. 13.
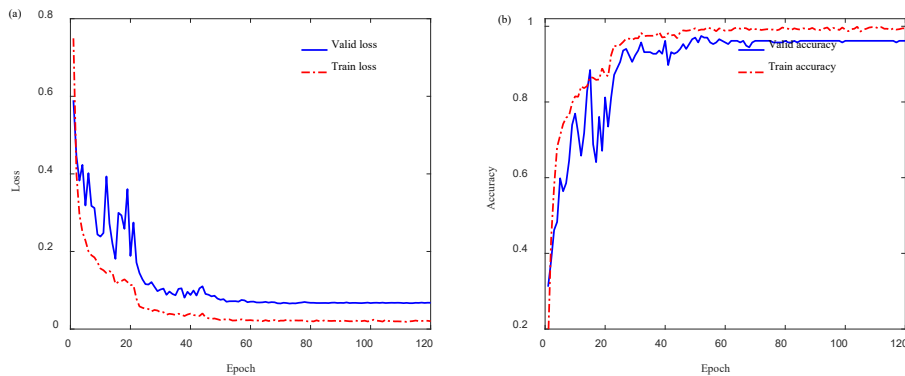

Figure 13. A training process using the Abnormal temperature data set (a) Loss (b) Accuracy

The training is repeated three times, and the mean value of validation accuracy was 95.31% with a standard deviation of 2.55%, as listed in Table 3. It can be seen that the classification accuracy is still high although the temperatures are not within the range of the training set. However, compared with the results of the Normal temperature

data set, the classification accuracy on the Abnormal temperature data set decreases slightly, and the standard deviation increases slightly. The compensated guided wave signals are compared with the uncompensated guided wave signals and the signals measured at the reference temperature, as shown in Fig. 14. Note that the temperatures at this time are outside the temperature range of the training data set.
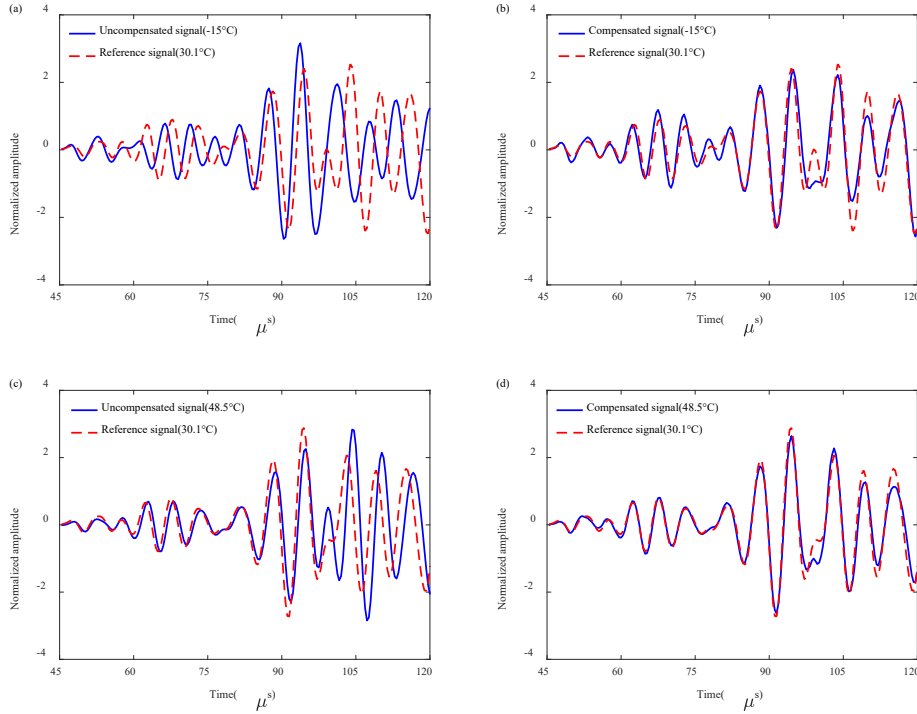

Figure 14 Temperature compensation results (a) uncompensated signal (-15.0°C) in loosening state 4 (b) compensated signal (-15.0°C) in loosening state 4 (c) uncompensated signal (48.5°C) in loosening state 10 (d) compensated signal (48.5°C) in loosening state 10.

As can be seen in Fig. 14, the compensated signals match well with the corresponding signals measured at the reference temperature. This proves that the proposed multi-task network has good generalization ability for temperature.

5.3 Comparison of classification results of different networks

To analyze the effect of the AG module on the classification results, the three AG modules are removed from the proposed network, and the network is named Unet_noAG. On the other hand, to verify the effect of the skip connection from the input to the Class-net, the skip connection is removed and it is named Unet_noskip.

Note that the AG module is retained at this time. The Unet_noAG and Unet_noskip were trained and validated by the three data sets. After three repetitions of training, the mean verification accuracy and standard deviations are listed in Table 3. The parameters of the networks are also listed in Table 3.

Table 3 Comparison of different neural networks

Networks	Normal temperature data set	Tightening batch data set	Abnormal temperature data set	Parameters
Unet_noAG	98.46%±1.07%	92.12%±1.40%	90.43%±4.63%	1,003,582
Unet_noskip	99.85%±0.27%	93.43%±2.59%	91.03%±1.13%	1,047,607
The proposed network	**100%**±0.00%	**95.60%**±1.37%	**95.31%**±2.55%	1,047,663
SHMnet	41.18%±2.27%	42.47%±0.42%	39.72%±1.23%	6,623,693

The results show that the classification accuracy decreases substantially on the three datasets after removing the AG modules, especially on the Tightening batch and the Abnormal temperature data sets. It can also be seen that there is only a small amount parameters in the AG modules. It can be concluded that the AG module can effectively improve the classification accuracy and the generalization ability of the network. Meanwhile, the classification accuracy decreases after removing the skip connection from the input to the Class-net, especially on the Tightening batch and the Abnormal temperature data sets.

The SHMnet, which is mainly consists of three convolutional layers and three fully connected layers, was also trained and validated by the three data sets and the results are listed in Table 3. The SHMnet directly performed loosening state identification according to the input guided wave signals without temperature compensation. It can be seen that the identification accuracy is low.

Figure 15a shows the difference signals between the guided waves of loosening states 4 and 13. Figure 15b shows the difference signals between loosening states 10 and 13. In the difference signal calculations, only one guided wave signal of loosening state 13 at the reference temperature was used. Two guided wave signals in loosening state 4 at different temperatures were used for the calculation. Similarly, the two signals in loosening state 10 were used. It can be seen that the difference signals change

significantly with temperature. Especially for loosening state 10, the change due to bolt loosening was completely covered by the change due to temperature. Therefore, if the classification is performed directly using CNNs without temperature compensation, it will cause a tremendous decrease in accuracy.
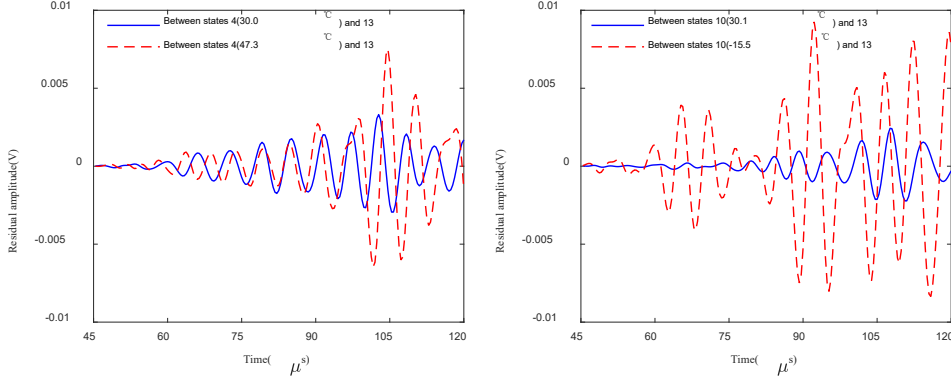

Figure 15. The difference signals (a) between signals of loosening states 4 and 13 (b) between signals of loosening states 10 and 13.

6．Interpretation of the model

It is important to understand the decisions of a deep network. The problem of attributing the predictions of the proposed multi-task network to its input feature of guided waves is investigated in this section. Given a specific target output, the goal of an attribution method is to determine the contribution of each input feature to the output. Hence, the Integrated Gradients method[57] is used to interpret the multi-task model. This method can be applied to a variety of deep networks, and has a strong theoretical justification. On this basis, the bolted joint is simplified and the effect of the direct guided wave on the classification results is discussed.

6.1 Interpretation by the Integrated Gradients method

The attribution of inputs can be created efficiently by directly computing the input gradient. The Integrated Gradients computes the path integral of the gradients along the straight-line path from the baseline to the input[58]. It can be expressed as

$$R_i^o(x) = (x_i - x_i') \int_{\gamma=0}^{1} \frac{\partial F(x' + \alpha(x - x'))}{\partial x_i} d\gamma \tag{7}$$

where x is input, x' is baseline, F is a function that represents the deep network, $\frac{\partial F(x)}{x_i}$ is the gradient of $F(x)$ along the ith dimension. The baseline is defined by the user and

often chosen to be zero.

The attribution of the input guided wave signal to the compensated guided wave signal was calculated. Note that the attribution can only be calculated for a single output point. For the result in Fig. 10, a target peak point in the compensated signal was selected and the attribution was calculated, as shown in Fig. 16. It can be seen that the target peak point after compensation depends mainly on the input peak point before time shift. Besides, the input signals which is far away from this input peak point have no contribution.
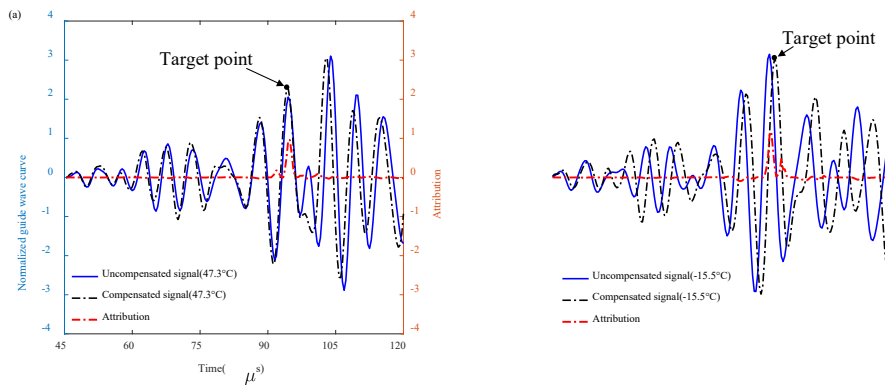

Figure 16. Attribution for the compensated signal (a)Loosening state 4 at temperature 47.3°C

(b)Loosening state 10 at temperature -15.5°C

Then, the Integrated Gradients method was used to attribute the classification output to its input. The input signal is the same as that in Fig. 16, and the attribution result is shown in Fig. 17. It can be seen that the classification of loosening states 4 and 10 is mainly based on the signal in the range of 60-105 μs. In addition, the attributions of the input signals before 60 μs and after about 110 μs are very small. The first direct S_0 wave packet is from 45 μs to about 60 μs. It is proved that the first S_0 wave packet is not sensitive for the contact area change due to bolt loosening. The reason should be that the in-plane displacement in the S_0 mode is dominant.
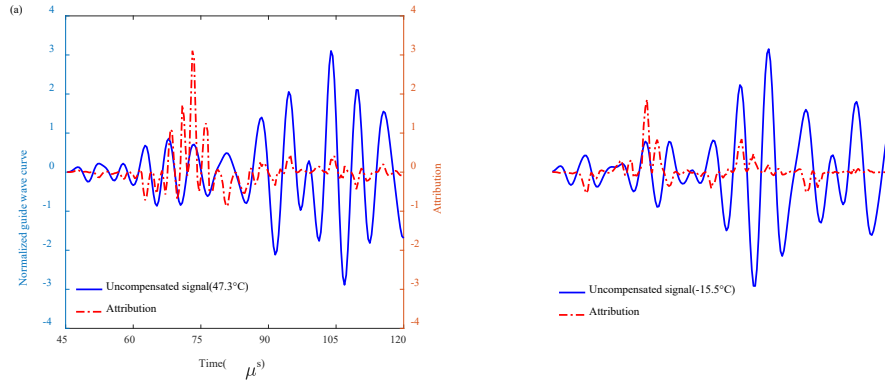
Figure 17. Attribution for the damage classification (a)Loosening state 4 at temperature 47.3°C (b) Loosening state 10 at temperature -15.5°C

6.2 Arrival time of the direct guided waves

The effect of the direct guided wave signals on the loosening state classification is further analyzed. Except for the first direct S_0 wave packet, other wave packets are difficult to separate due to the superposition of each other. To this end, the bolted joint was simplified, as shown in Fig. 18. It is assumed that the lapped plates between positions 1 and 2 is in full contact, while the rest of the part is not in contact. Positions 1 and 2 are determined according to the half-apex angle of the bolt, which is chosen to be $\theta = 45°$[48]. Thus the bolt lap plate is divided into regions I, II and III. The mode conversions at positions 1 and 2 are considered. The reflected waves and the bolt holes are not taken into account.
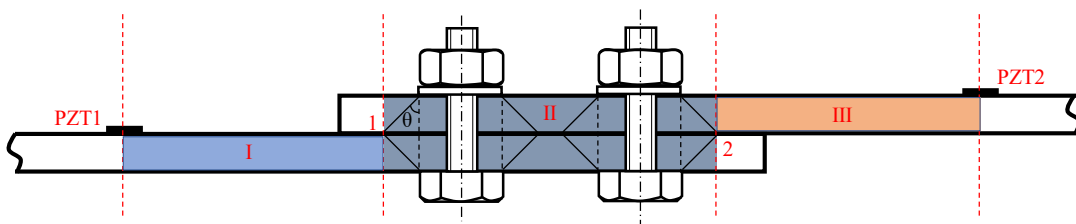
Figure 18 Schematic diagram of simplified structure of the bolt lap plate

Then, the arrival times of different direct guided waves were calculated. There are 8 mode conversion cases for the direct arrival waves, as listed in Table 4. For example, S_0-A_0-S_0 indicates that the mode in region I is S_0, the mode in region II is A_0, and the mode in region III is S_0. The arrival times of these direct wave packets were calculated using group velocity, and the results are listed in Table 4.

Table 4 Arrival time of the direct guide wave

No.	Models of the direct arrival wave	Arrival time(μs)
1	S_0-S_0-S_0	43.67
2	S_0-A_0-S_0	50.85
3	S_0-S_0-A_0	56.99
4	A_0-S_0-S_0	56.99
5	S_0-A_0-A_0	64.17
6	A_0-A_0-S_0	64.17
7	A_0-S_0-A_0	70.32
8	A_0-A_0-A_0	77.50

It can be seen that the arrival times of the direct wave packets are between 43.67-77.5 μs, while the excitation signal width is 17.5 μs. For the direct arrival wave packet S_0-S_0-S_0, the width is consistent with the excitation signal, so the wave packet is in the time interval of 43.67-61.17 μs. This is consistent with the time range of the first direct S_0 wave packet obtained from the experimental signals shown in Fig. 10. It is proved that the simplification shown in Fig. 18 is feasible.

For the direct arrival wave packet A_0-A_0-A_0, the time interval is from 77.50 μs to about 95 μs. Note that the wave packet length should be longer than 17.5 μs because of the dispersion of the A_0 mode. There is a large decrease in the attribution after 105 μs as shown in Fig. 17. It can be deduced that the reflected wave is not sensitive to bolt loosening. Furthermore, the direct S_0-S_0-S_0 is not sensitive to bolt loosening. It can be concluded that the direct arrival waves that have contained the A_0 mode are sensitive to bolt loosening and should be selected for bolt loosening identification.

From Figs. 7, it can be seen that the signal of 25 μs length contains the S_0-S_0-S_0 and part of the S_0-A_0-S_0 packet. At this time, the signal values which are more sensitive to classification cannot be utilized, resulting in low accuracy of bolt loosening recognition. For the 100 μs length signal, it contains more reflected wave signals after the A_0-A_0-A_0. At this point, the increased signal length which has low sensitivity for classification may cause interference, resulting in a slight decrease in classification

accuracy. It can be concluded that the proposed simplified structure can be used for the selection of input signal length for bolt loosening detection.

7. Conclusions

(1) An attention-based multi-task neural network is developed for temperature compensation and bolt loosening detection using guided waves. By integrating improved AG modules in a modified U-Net architecture, a 1D attention U-Net (Comp-net) is established for temperature compensation. Then a two-layer convolutional subnetwork (Class-net) is connected in series behind the Comp-net to identify bolt loosening. Moreover, a skip connection is used to concatenate from the input to the Class-net. A loss function composed of mean squared error loss, total variation regularizer and cross-entropy loss is used.

(2) Experiment validation is carried out on a bolt jointed lap plate simulating a real aircraft structure. Two PZTs were used to monitor the tightening toques of six bolts over a wide range of temperature variation. The results have proved that the developed multi-task network achieves temperature compensation and accurate bolt loosening identification. The AG modules and skip connection have significant effects on the classification accuracy and the generalization ability of the model. Besides, there is a tremendous decrease in accuracy without temperature compensation in advance.

(3) The generalization capabilities for tightening batches and temperatures of the proposed multi-task network are verified. When the temperatures and tightening batches are not within the range of the training set, the classification accuracy decreases little.

(4) The Integrated Gradients method and a simplified structure of the bolt lap plate are used to interpret the multi-task network. The attributions of inputs to the outputs were calculated by the Integrated Gradients method. The arrival times of different direct guided wave packet were estimate by the simplified structure. It has been proven that the direct arrival wave of S_0 mode and the reflected waves are not sensitive for the contact area change due to bolt loosening. In addition, the direct arrival wave of the A_0 mode is sensitive to bolt loosening and should be selected for bolt loosening

identification. In addition, the simplified structure is helpful for the selection of input signal length.

The PZT transducers are glued to the structure in this study, which may lead to inconvenience in some engineering applications. Therefore, the importance of automatic strategies such as the robotic-assisted active sensing method for bolt looseness detection has been noticed, this could be a future direction.

Acknowledgments

References

1. Wang F and Song G. 1D-TICapsNet: An audio signal processing algorithm for bolt early looseness detection. *Structural Health Monitoring* 2020. DOI: 10.1177/1475921720976989.

2. Sun H, Wang T, Liu Q, et al. A two-dimensional eddy current array— based sensing film for estimating failure modes and tracking damage growth of bolted joints. *Structural Health Monitoring* 2019; 20: 877-893. DOI: 10.1177/1475921719843062.

3. Zhang Z, Xiao Y, Su Z, et al. Continuous monitoring of tightening condition of single-lap bolted composite joints using intrinsic mode functions of acoustic emission signals: a proof-of-concept study. *Structural Health Monitoring* 2018; 18: 1219-1234. DOI: 10.1177/1475921718790768.

4. Zhu Y, Li F and Hu Y. The contact characteristics analysis for rod fastening

rotors using ultrasonic guided waves. *Measurement* 2020; 151. DOI: 10.1016/j.measurement.2019.107149.

5. Zeng L, Huang L, Cao X, et al. Determination of Lamb wave phase velocity dispersion using time–frequency analysis. *Smart Materials and Structures* 2019; 28. DOI: 10.1088/1361-665X/ab47e1.

6. Cai J, Wang X and Zhou Z. A signal domain transform method for spatial resolution improvement of Lamb wave signals with synthetically measured relative wavenumber curves. *Structural Health Monitoring* 2018; 18: 1633-1651. DOI: 10.1177/1475921718807310.

7. Du F, Xu C, Ren H, et al. Structural health monitoring of bolted joints using guided waves: a review. In: Magd Abdel Wahab, Yun Lai Zhou and Maia NMM (eds) *Structural Health Monitoring from Sensing to Processing*. London, SW7 2QJ, UNITED KINGDOM: IntechOpen, 2018, pp.163-180.

8. Yang J and Chang F-K. Detection of bolt loosening in C–C composite thermal protection panels: I. Diagnostic principle. *Smart Materials and Structures* 2006; 15: 581-590. DOI: 10.1088/0964-1726/15/2/041.

9. Wang T, Song G, Wang Z, et al. Proof-of-concept study of monitoring bolt connection status using a piezoelectric based active sensing method. *Smart Materials and Structures* 2013; 22: 087001.

10. Haynes C, Yeager M, Todd M, et al. Monitoring bolt torque levels through signal processing of full-field ultrasonic data. In: *Health Monitoring of Structural and Biological Systems 2014* 2014, p.906428. International

Society for Optics and Photonics.

11. Mascarenas D, Macknelly D, Mullins J, et al. Dynamic characterization of satellite assembly for responsive space applications. *Measurement Science and Technology* 2013; 24: 075101.

12. Montoya A, Doyle D, Maji A, et al. Ultrasonic Evaluation of Bolted Connections in Satellites. *Research in Nondestructive Evaluation* 2014; 25: 44-62.

13. Jiang T, Wu Q, Wang L, et al. Monitoring of Bolt Looseness-Induced Damage in Steel Truss Arch Structure Using Piezoceramic Transducers. *Ieee Sens J* 2018; 18: 6677-6685.

14. Du F, Xu C and Zhang J. A bolt preload monitoring method based on the refocusing capability of virtual time reversal. *Structural Control and Health Monitoring* 2019. DOI: 10.1002/stc.2370.

15. Wang F, Ho SCM and Song G. Monitoring of early looseness of multi-bolt connection: a new entropy-based active sensing method without saturation. *Smart Materials and Structures* 2019; 28. DOI: 10.1088/1361-665X/ab3a08.

16. Parvasi SM, Ho SCM, Kong Q, et al. Real time bolt preload monitoring using piezoceramic transducers and time reversal technique—a numerical study with experimental verification. *Smart Materials and Structures* 2016; 25: 085015.

17. Mitra M and Gopalakrishnan S. Guided wave based structural health

monitoring: A review. *Smart Materials and Structures* 2016; 25: 053001. DOI: 10.1088/0964-1726/25/5/053001.

18. Lu Y and Michaels JE. A methodology for structural health monitoring with diffuse ultrasonic waves in the presence of temperature variations. *Ultrasonics* 2005; 43: 717-731. 2005/07/05. DOI: 10.1016/j.ultras.2005.05.001.

19. Konstantinidis G, Drinkwater BW and Wilcox PD. The temperature stability of guided wave structural health monitoring systems. *Smart Materials and Structures* 2006; 15: 967-976. DOI: 10.1088/0964-1726/15/4/010.

20. An Y-K and Sohn H. Integrated impedance and guided wave based damage detection. *Mechanical Systems and Signal Processing* 2012; 28: 50-62. DOI: 10.1016/j.ymssp.2011.11.016.

21. Clarke T, Simonetti F and Cawley P. Guided wave health monitoring of complex structures by sparse array systems: Influence of temperature changes on performance. *Journal of Sound and Vibration* 2010; 329: 2306-2322.

22. Kundu T, Croxford AJ, Wilcox PD, et al. Strategies for overcoming the effect of temperature on guided wave structural health monitoring. *Health Monitoring of Structural and Biological Systems 2007*. 2007.

23. Mariani S, Heinlein S and Cawley P. Compensation for temperature-dependent phase and velocity of guided wave signals in baseline

subtraction for structural health monitoring. *Structural Health Monitoring* 2019: 147592171983515. DOI: 10.1177/1475921719835155.

24. Yue N and Aliabadi MH. A scalable data-driven approach to temperature baseline reconstruction for guided wave structural health monitoring of anisotropic carbon-fibre-reinforced polymer structures. *Structural Health Monitoring* 2019. DOI: 10.1177/1475921719887109.

25. Gorgin R, Luo Y and Wu Z. Environmental and operational conditions effects on Lamb wave based structural health monitoring systems: A review. *Ultrasonics* 2020; 105: 106114. 2020/03/21. DOI: 10.1016/j.ultras.2020.106114.

26. Nazarko P and Ziemianski L. Force identification in bolts of flange connections for structural health monitoring and failure prevention. *Procedia Structural Integrity* 2017; 5: 460-467. DOI: 10.1016/j.prostr.2017.07.142.

27. Liang D and Yuan S-f. Decision fusion system for bolted joint monitoring. *Shock and Vibration* 2015; 2015.

28. Wang F, Chen Z and Song G. Monitoring of multi-bolt connection looseness using entropy-based active sensing and genetic algorithm-based least square support vector machine. *Mechanical Systems and Signal Processing* 2020; 136. DOI: 10.1016/j.ymssp.2019.106507.

29. Wang F, Chen Z and Song G. Smart crawfish: A concept of underwater multi-bolt looseness identification using entropy-enhanced active sensing

and ensemble learning. *Mechanical Systems and Signal Processing* 2021; 149. DOI: 10.1016/j.ymssp.2020.107186.

30. Ying Y, Garrett JH, Oppenheim IJ, et al. Toward Data-Driven Structural Health Monitoring: Application of Machine Learning and Signal Processing to Damage Detection. *Journal of Computing in Civil Engineering* 2013; 27: 667-680. DOI: 10.1061/(asce)cp.1943-5487.0000258.

31. Wang P, Zhou W, Bao Y, et al. Ice monitoring of a full-scale wind turbine blade using ultrasonic guided waves under varying temperature conditions. *Structural Control and Health Monitoring* 2018; 25: e2138. DOI: 10.1002/stc.2138.

32. LeCun Y, Bengio Y and Hinton G. Deep learning. *Nature* 2015; 521: 436-444. 2015/05/29. DOI: 10.1038/nature14539.

33. Zhu J, Chen N and Shen C. A New Deep Transfer Learning Method for Bearing Fault Diagnosis Under Different Working Conditions. *Ieee Sens J* 2020; 20: 8394-8402. DOI: 10.1109/jsen.2019.2936932.

34. Li J, Wang Y, Zi Y, et al. Whitening-Net: A Generalized Network to Diagnose the Faults Among Different Machines and Conditions. *IEEE Trans Neural Netw Learn Syst* 2021; PP 2021/04/23. DOI: 10.1109/TNNLS.2021.3071564.

35. Bukhsh ZA, Jansen N and Saeed A. Damage detection using in-domain and cross-domain transfer learning. *Neural Computing and Applications* 2021; 33: 16921-16936. DOI: 10.1007/s00521-021-06279-x.

36. Iyer S, Velmurugan T, Gandomi AH, et al. Structural health monitoring of railway tracks using IoT-based multi-robot system. *Neural Computing and Applications* 2020; 33: 5897-5915. DOI: 10.1007/s00521-020-05366-9.

37. Yang S and Huang Y. Damage identification method of prestressed concrete beam bridge based on convolutional neural network. *Neural Computing and Applications* 2020; 33: 535-545. DOI: 10.1007/s00521-020-05052-w.

38. Zhang Y, Sun X, Loh KJ, et al. Autonomous bolt loosening detection using deep learning. *Structural Health Monitoring* 2019; 19: 105-122. DOI: 10.1177/1475921719837509.

39. Wang F. A novel autonomous strategy for multi-bolt looseness detection using smart glove and Siamese double-path CapsNet. *Structural Health Monitoring* 2021. DOI: 10.1177/14759217211054575.

40. Zhang T, Biswal S and Wang Y. SHMnet: Condition assessment of bolted connection with beyond human-level performance. *Structural Health Monitoring* 2019; 19: 1188-1201. DOI: 10.1177/1475921719881237.

41. Zhang B, Hong X and Liu Y. Multi-task deep transfer learning method for guided wave based integrated health monitoring using piezoelectric transducers. *Ieee Sens J* 2020: 1-1. DOI: 10.1109/jsen.2020.3009194.

42. Vaswani A, Shazeer N, Parmar N, et al. Attention is all you need. In: *Proceedings of the 31st International Conference on Neural Information Processing Systems* 2017, pp.6000-6010.

43. Jetley S, Lord NA, Lee N, et al. Learn to Pay Attention. In: *International Conference on Learning Representations* 2018.

44. Fu J, Liu J, Tian H, et al. Dual attention network for scene segmentation. In: *Proceedings of the IEEE/CVF Conference on Computer Vision and Pattern Recognition* 2019, pp.3146-3154.

45. Oktay O, Schlemper J, Folgoc LL, et al. Attention u-net: Learning where to look for the pancreas. *arXiv preprint arXiv:180403999* 2018.

46. Abraham N and Khan NM. A novel focal tversky loss function with improved attention u-net for lesion segmentation. In: *2019 IEEE 16th International Symposium on Biomedical Imaging (ISBI 2019)* 2019, pp.683-687. IEEE.

47. Zhang H, Goodfellow I, Metaxas D, et al. Self-attention generative adversarial networks. In: *International conference on machine learning* 2019, pp.7354-7363. PMLR.

48. Oskouei RH, Keikhosravy M and Soutis C. Estimating clamping pressure distribution and stiffness in aircraft bolted joints by finite-element analysis. *Proceedings of the Institution of Mechanical Engineers, Part G: Journal of Aerospace Engineering* 2009; 223: 863-871. DOI: 10.1243/09544100jaero596.

49. Huda F, Kajiwara I, Hosoya N, et al. Bolt loosening analysis and diagnosis by non-contact laser excitation vibration tests. *Mechanical Systems and Signal Processing* 2013; 40: 589-604. DOI: 10.1016/j.ymssp.2013.05.023.

50. Kedra R and Rucka M. Research on assessment of bolted joint state using elastic wave propagation. *Journal of Physics: Conference Series* 2015; 628: 012025.

51. Amerini F and Meo M. Structural health monitoring of bolted joints using linear and nonlinear acoustic/ultrasound methods. *Structural Health Monitoring* 2011; 10: 659-672.

52. Croxford AJ, Moll J, Wilcox PD, et al. Efficient temperature compensation strategies for guided wave structural health monitoring. *Ultrasonics* 2010; 50: 517-528. 2009/12/25. DOI: 10.1016/j.ultras.2009.11.002.

53. Croxford AJ, Wilcox PD, Drinkwater BW, et al. Strategies for guided-wave structural health monitoring. *Proceedings of the Royal Society A: Mathematical, Physical and Engineering Sciences* 2007; 463: 2961-2981. DOI: 10.1098/rspa.2007.0048.

54. Du F, Wu S, Xu C, et al. Electromechanical impedance temperature compensation and bolt loosening monitoring based on modified Unet and multitask learning. *Ieee Sens J* 2021. DOI: 10.1109/JSEN.2021.3132943.

55. Fang Y, Ma Z, Zhang Z, et al. Dynamic Multi-Task Learning with Convolutional Neural Network. *Proceedings of the Twenty-Sixth International Joint Conference on Artificial Intelligence*. 2017, p. 1668-1674.

56. Guo S, Yan Z, Zhang K, et al. Toward convolutional blind denoising of real photographs. In: *Proceedings of the IEEE/CVF Conference on Computer*

Vision and Pattern Recognition 2019, pp.1712-1722.

57. Sundararajan M, Taly A and Yan Q. Axiomatic Attribution for Deep Networks. In: Doina P and Yee Whye T, (eds.). *Proceedings of the 34th International Conference on Machine Learning*. Proceedings of Machine Learning Research: PMLR, 2017, p. 3319--3328.

58. Ancona M, Ceolini E, Öztireli C, et al. Towards better understanding of gradient-based attribution methods for Deep Neural Networks. In: *6th International Conference on Learning Representations, ICLR 2018, Vancouver, BC, Canada, April 30-May 3, 2018, Conference Track Proceedings* 2018, OpenReview. net.